JOURNAL OF GUIDANCE, CONTROL, AND DYNAMICS
Vol. 20, No. 2, March–April 1997

Stability of a Spinning Axisymmetric Rocket with Dissipative Internal Mass Motion

Y. Yam*
Chinese University of Hong Kong, Shatin, New Territories, Hong Kong
D. L. Mingori†
University of California, Los Angeles, Los Angeles, California 90095-1597
and
D. M. Halsmer‡
Oral Roberts University, Tulsa, Oklahoma 74171

One hypothesis for explaining the coning instabilities observed in certain spinning axisymmetric solid fuel rockets attributes the source of the instability to the accumulation of slag near the exit of the rocket casing. Previously this hypothesis was explored using a particle model with elastic restoring forces to represent the slag motion. A recent paper further examines how the results are modified when dissipative forces are added to the model. The work is based on the second method of Lyapunov. An alternative derivation of the dissipative results is now provided. The new derivation is based on perturbation analysis of the undamped characteristic values and yields additional insight into the stability results. A numerical example simulating the coning instability is also given. It shows that a coning growth similar to that observed in space is possible assuming certain time histories of spacecraft parameters. The example requires the natural frequency of moving mass to be close to the nominal spacecraft spin rate to produce the coning instability. In addition to their relevance for the specific problem of spinning rocket stability, the results presented provide insight on how the maximum axis spin rule for torque free spinning bodies is modified in the presence of thrust.

Introduction

IN the early to mid-1980s, coning instabilities were observed on certain transfer orbit boost vehicles such as the Perigee Assist Module-D. These instabilities occurred near the end of the burn of a solid rocket engine. Several hypotheses were advanced to explain this phenomenon, but most were eliminated by detailed comparison with flight data. Two remain under active consideration, one that attributes the instability to gas dynamics in the combustion chamber[1] and one that attributes the instability to the interaction between the thrust vector and the internal motion of combustion products (slag) in the rocket motor casing.[2] A universally accepted explanation does not appear to exist. This paper focuses on the latter (slag) hypothesis.

The slag hypothesis was first analyzed in Ref. 2 with an elastic moving mass model. The results show that rapid coning growth similar to that observed in space can occur if the thrust magnitude is sufficiently large and the moving mass is aft of the system mass center. In Ref. 3, the effects on a spinning rocket of either a single spherical pendulum model or a pair of planar pendula were studied. It was suggested that actual liquid sloshing may have a qualitative force balance that is a combination of these two types of pendulum models. An idealized model subsequently constructed to reflect this force balance was able to demonstrate the coning instability. The issue was further pursued in Ref. 4, where the effect of sloshing was analyzed with a linearized hydrodynamic coupled finite element model. The work shows that coning instability can occur due to coupling between the spacecraft nutation and one of the swirl modes of the liquid. This contrasts a previous work, which investigated a hydrodynamic model under a different set of conditions and produced no instability.[5] Another work involving basically a one-dimensional fluid model is given in Ref. 6. The works of Refs. 2–6 apply linearized analysis to the dynamical equations. Nonlinear treatments of the problem involving mechanical models are given in Refs. 7 and 8. The nonlinear analysis enhances simulation of the spacecraft motion under some restrictions.

The aforementioned works assume nondissipative slag models in their analysis. The development in Ref. 2 focuses on a spinning symmetric spacecraft model with axial thrust and purely elastic internal mass motion (no damping). The point was made that the instabilities identified did not rely on damping or the presence of internal energy dissipation. The result is in marked contrast to previous studies of freely spinning bodies without thrust. The extensive research during the late 1950s and 1960s focusing on the question of how dissipative internal mass motion affects the coning stability of freely spinning spacecraft have led to the maximum axis spin rule for simple spinners and the dual spin stability inequality for dual spinners.[9] A recent work contains a detailed analysis of the effect of a precession damper on the motion of a torque free spinning body.[10] The work focuses on the unstable dynamics and shows that the apparent limit cycles are actually transient motions slowly decaying to an equilibrium. For the torque free coning problem, stability results with dissipative forces added to the internal mass model were investigated in Ref. 11 using the second method of Lyapunov. The results show that regions that were unstable in the absence of dissipative forces remain so when damping is added. In areas where the undamped stability results were inconclusive, some regions become unstable and some become asymptotically stable. Thus, the region of instability in the presence of dissipative forces is larger than that found for purely elastic forces.

In this paper, an alternate derivation of the dissipative results in Ref. 11 is provided. The new derivation is based on the complex variable formulation of Ref. 2 followed by a perturbation analysis of the undamped characteristic values. The results provide additional insight into the stability conditions. The present paper also gives a numerical example simulating the coning instability. It shows that a coning growth similar to that observed in space is possible assuming certain time histories of spacecraft parameters. The example requires the internal mass to have a natural frequency close to the nominal spin rate of the spacecraft to produce the coning instability.

Received Oct. 17, 1995; revision received Oct. 31, 1996; accepted for publication Nov. 11, 1996.

*Associate Professor, Department of Mechanical and Automation Engineering.
†Professor, Mechanical, Aerospace, and Nuclear Engineering Department. Associate Fellow AIAA.
‡Assistant Professor of Engineering. Member AIAA.

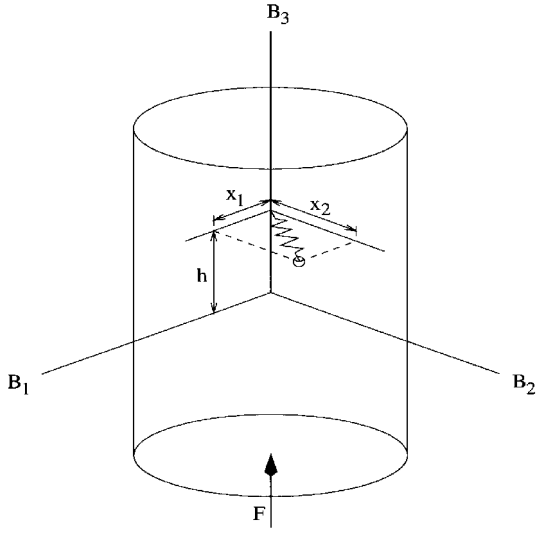

Fig. 1 Idealized spacecraft model.

Model

The model used in this investigation is shown in Fig. 1. It consists of a symmetric rigid body containing a mass particle, which can move in a plane perpendicular to the symmetric axis. The axes B_1, B_2, and B_3 are fixed in the rigid body and pass through the point coinciding with system mass center when x_1 and x_2 are zero. Nominally the particle is on the B_3 axis a distance h from the system mass center. Motion of the particle away from the axis produces a linear elastic restoring force with spring constant k and a linear damping force with damping constant c. A thrust vector with magnitude F acts along the symmetry axis and passes through the mass center of the rigid body. The thrust vector is a nonconservative force of a type sometimes called a follower force in the literature.[12] This model is identical to that considered in Ref. 2 except that motion of the internal mass is here assumed to produce dissipative as well as elastic forces.

The particle represents internal mass motion in the rocket. A primary source for such motion is the liquified slag, which collects in the aft portion of the rocket engine as a byproduct of the burning solid fuel. Clearly, a particle model fails to capture many phenomena a sloshing fluid can exhibit. However, a simple particle model does include the major first-order effect of liquid motion and provides a preliminary understanding of the resulting dynamics.

Governing Equations

Four real (or two complex) coupled linear differential equations are required to describe the coning motion of the spacecraft for small cone angles. The first two of the real equations may be obtained from the angular momentum principle. For small cone angles, the system angular momentum for the system mass center may be approximated as

$$\boldsymbol{H}_c = \left(I_1 + mh^2\right)\omega_1 \boldsymbol{b}_1 + \left(I_1 + mh^2\right)\omega_2 \boldsymbol{b}_2 + I_3 \Omega \boldsymbol{b}_3 - mh(\dot{x}_2 + x_1\Omega)\boldsymbol{b}_1 + mh(\dot{x}_1 - x_1\Omega)\boldsymbol{b}_2 \tag{1}$$

The externally applied torque due to the thrust vector $F\boldsymbol{b}_3$ is

$$\boldsymbol{M}_c = -\mu F x_2 \boldsymbol{b}_1 + \mu F x_1 \boldsymbol{b}_2 \tag{2}$$

In Eqs. (1) and (2),

ω_1, ω_2	=	components of the rigid-body angular velocity for the axes B_1 and B_2, respectively.
$\boldsymbol{b}_1, \boldsymbol{b}_2, \boldsymbol{b}_3$	=	body-fixed unit vectors parallel to the axes B_1, B_2, and B_3, respectively.
I_1, I_1, I_3	=	moments of inertia of the (symmetric) rigid body for the axes B_1, B_2, and B_3, respectively.
m	=	mass of particle
M	=	mass of rigid body
μ	=	$m/(m+M)$
F	=	magnitude of thrust (assumed constant)
Ω	=	nominal spin rate of rigid body about B_3
t	=	independent variable (time)

Variables not defined in the preceding list are defined in Fig. 1.

Applying the angular momentum principle, $\mathrm{d}\boldsymbol{H}_c/\mathrm{d}t = \boldsymbol{M}_c$, and taking the $\boldsymbol{b}_1$ and $\boldsymbol{b}_2$ components of the result leads to

$$\left(I_1 + mh^2\right)\dot{\omega}_1 + \left[I_3 - \left(I_1 + mh^2\right)\right]\Omega\omega_2 = 2\Omega mh\dot{x}_1 + mh\ddot{x}_2 - mh\Omega^2 x_2 - \mu F x_2 \tag{3}$$

$$\left(I_1 + mh^2\right)\dot{\omega}_2 - \left[I_3 - \left(I_1 + mh^2\right)\right]\Omega\omega_1 = 2\Omega mh\dot{x}_2 - mh\ddot{x}_1 + mh\Omega^2 x_1 + \mu F x_1 \tag{4}$$

where the over dot denotes differentiation with respect to the time variable t. Equations (3) and (4) represent the first two governing equations in real form. The second two equations may be obtained by applying Newton's second law to the particle and taking the components of the result in the $\boldsymbol{b}_1$ and $\boldsymbol{b}_2$ directions. For small cone angles, the $\boldsymbol{b}_1$ and $\boldsymbol{b}_2$ components of the particle acceleration $\boldsymbol{a}$ may be expressed as

$$\boldsymbol{a}\cdot\boldsymbol{b}_1 = (1-\mu)\left(\ddot{x}_1 - 2\Omega\dot{x}_2 - \Omega^2 x_1\right) + h(\dot{\omega}_2 + \Omega\omega_1) \tag{5}$$

$$\boldsymbol{a}\cdot\boldsymbol{b}_2 = (1-\mu)\left(\ddot{x}_2 + 2\Omega\dot{x}_1 - \Omega^2 x_2\right) + h(-\dot{\omega}_1 + \Omega\omega_2) \tag{6}$$

The $\boldsymbol{b}_1$ and $\boldsymbol{b}_2$ component of the force $\boldsymbol{f}$ applied to the particle may be expressed as

$$\boldsymbol{f}\cdot\boldsymbol{b}_1 = -kx_1 - c\dot{x}_1 \tag{7}$$

$$\boldsymbol{f}\cdot\boldsymbol{b}_2 = -kx_2 - c\dot{x}_2 \tag{8}$$

where

k = spring constant for elastic restraint on the particle
c = damping constant for the particle motion

From Newton's second law, i.e., $\boldsymbol{f}\cdot\boldsymbol{b}_i = m\boldsymbol{a}\cdot\boldsymbol{b}_i$, $i = 1, 2$, we obtained the second two governing equations in real form,

$$-kx_1 - c\dot{x}_1 = m\left[(1-\mu)\left(\ddot{x}_1 - 2\Omega\dot{x}_2 - \Omega^2 x_1\right) + h(\dot{\omega}_2 + \Omega\omega_1)\right] \tag{9}$$

$$-kx_2 - c\dot{x}_2 = m\left[(1-\mu)\left(\ddot{x}_2 + 2\Omega\dot{x}_1 - \Omega^2 x_2\right) + h(-\dot{\omega}_1 + \Omega\omega_2)\right] \tag{10}$$

Before attempting to analyze these equations, it is convenient to define some new parameters and variables. Let

$$\lambda = \frac{\left\{I_3 - I_1 + [\mu mh^2/(1-\mu)]\right\}}{\left\{I_1 - [\mu mh^2/(1-\mu)]\right\}} \tag{11}$$

$$\gamma^2 = \frac{k}{m(1-\mu)\Omega^2} \tag{12}$$

$$\xi = \frac{c}{m(1-\mu)\Omega} \tag{13}$$

$$y_i = \frac{(1-\mu)x_i}{|h|} \tag{14}$$

$$\delta = \frac{mh^2}{(1-\mu)\left\{I_1 - [\mu mh^2/(1-\mu)]\right\}} \tag{15}$$

$$T = \frac{\mu hF}{(1-\mu)\Omega^2\left\{I_1 - [\mu mh^2/(1-\mu)]\right\}} \tag{16}$$

$$r = |h|/h = \pm 1 \tag{17}$$

Using these dimensionless quantities and substituting $\ddot{x}_1$ and $\ddot{x}_2$ from Eqs. (9) and (10) into the right-hand side of Eqs. (3) and (4) yields the governing equations in the following form:

$$\dot{\omega}_1 + \lambda\Omega\omega_2 = -r(\delta\gamma^2 + T)\Omega^2 y_2 - r\delta\xi\Omega\dot{y}_2 \tag{18}$$

$$\dot{\omega}_2 - \lambda\Omega\omega_1 = r(\delta\gamma^2 + T)\Omega^2 y_1 + r\delta\xi\Omega\dot{y}_1 \tag{19}$$

$$\ddot{y}_1 - 2\Omega\dot{y}_2 + (\gamma^2 - 1)\Omega^2 y_1 + \xi\Omega\dot{y}_1 = -r(\dot{\omega}_2 + \Omega\omega_1) \tag{20}$$

$$\ddot{y}_2 + 2\Omega\dot{y}_1 + (\gamma^2 - 1)\Omega^2 y_2 + \xi\Omega\dot{y}_2 = r(\dot{\omega}_1 - \Omega\omega_2) \tag{21}$$

Equations (18–21) can be written in complex form by defining $\omega = \omega_1 + j\omega_2$ and $y = y_1 + jy_2$. Thus,

$$\dot{\omega} - j\lambda\Omega\omega = jr(\delta\gamma^2 + T)\Omega^2 y + jr\delta\xi\Omega\dot{y} \tag{22}$$

$$\ddot{y} + j2\Omega\dot{y} + (\gamma^2 - 1)\Omega^2 y + \xi\Omega\dot{y} = r(j\dot{\omega} - \Omega\omega) \tag{23}$$

Further simplification is possible with the introduction of additional dimensionless quantities. Let

$$\Lambda = 1 + \lambda \tag{24}$$

$$\Delta = 1 + \delta \tag{25}$$

$$\tau = \Omega\Lambda t \tag{26}$$

$$u = \frac{\omega e^{j(\tau/\Lambda)}}{\Omega\Lambda} \tag{27}$$

$$z = ye^{j(\tau/\Lambda)} \tag{28}$$

$$T_o = \frac{\delta\gamma^2 + T}{\Lambda^2} \tag{29}$$

$$\xi_o = \xi\Delta/\Lambda \tag{30}$$

$$\beta^2 = \gamma^2/\Lambda^2 \tag{31}$$

Then Eqs. (22) and (23) reduce to

$$u' - ju = jrT_o z + r\delta\xi_o(z/\Lambda + jz')/\Delta \tag{32}$$

$$z'' + \beta^2 z = jru' + j\xi_o(z/\Lambda + jz')/\Delta \tag{33}$$

where the prime superscript denotes differentiation with respect to τ. Equations (32) and (33) are now in a very convenient form for analysis.

Stability Analysis

Writing Eqs. (32) and (33) in Laplace transform notation yields

$$\begin{bmatrix} (s-j) & -jrT_o - r\delta\xi_o(1/\Lambda + js)/\Delta \\ -jrs & s^2 + \beta^2 - j\xi_o(1/\Lambda + js)/\Delta \end{bmatrix} \begin{bmatrix} u(s) \\ z(s) \end{bmatrix} = 0 \tag{34}$$

The characteristic equation for this system is

$$(s-j)(s^2+\beta^2)+T_o s - j\xi_o(1/\Lambda+js)[(s-j)+s\delta]/\Delta = 0 \tag{35}$$

Let $s = -jq$. The characteristic equation then becomes

$$(q+1)(q^2-\beta^2) - T_o q + j\xi_o(q+1/\Lambda)(q+1/\Delta) = 0 \tag{36}$$

When the roots of Eq. (36) have negative imaginary parts, the roots of Eq. (35) have negative real parts indicating stability. Denote $C_o(q) = (q+1)(q^2-\beta^2) - T_o q$, and Eq. (36) becomes

$$C_o(q) + j\xi_o(q+1/\Lambda)(q+1/\Delta) = 0 \tag{37}$$

Undamped Case: $\xi_o = 0$

The characteristic equation reduces to one with real coefficients,

$$C_o(q) = (q+1)(q^2-\beta^2) - T_o q = 0 \tag{38}$$

The roots of Eq. (38) are either all real, indicating marginal stability, or they contain a complex conjugate pair, indicating instability. The boundary between stability and instability occurs when Eq. (38) has two equal roots. To find the condition for equal roots, write Eq. (38) in a form suitable for root locus analysis,

$$1 + \frac{(-T_o)q}{(q+1)(q+\beta)(q-\beta)} = 0 \tag{39}$$

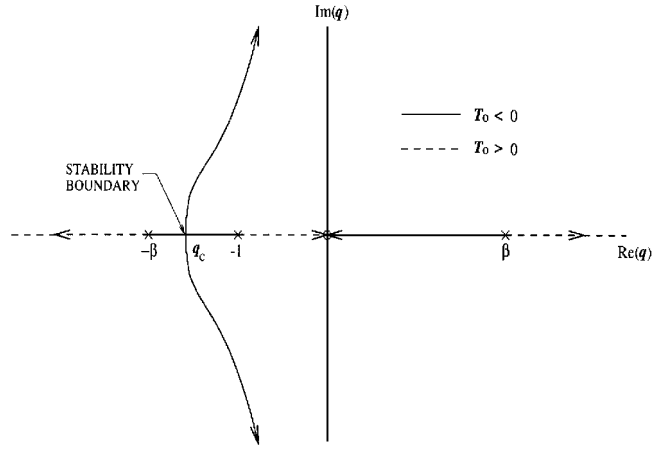

Fig. 2 Root locus for $C_o(q) = 0$.

Figure 2 shows the locus of roots of Eq. (39) as T_o is varied. Note that instability can only occur for $T_o < 0$. As $T_o = \delta\beta^2 + T/\Lambda^2$ and $\delta \geq 0$, this means T must be negative, and hence, h must be negative. Therefore, this instability can only occur if the moving internal mass is aft of the system mass center.

To locate the breakaway point q_c and corresponding value of T_o, solve Eq. (38) for T_o:

$$T_o = \frac{(q+1)(q^2-\beta^2)}{q} \tag{40}$$

At breakaway, $dT_o/dq = 0$. Thus,

$$2q^3 + q^2 + \beta^2 = 0 \tag{41}$$

To solve this equation, let $p = 1/q$. Then,

$$p^3 + p/\beta^2 + 2/\beta^2 = 0 \tag{42}$$

Using standard formulas for cubic polynomials, the roots of Eq. (42) are $p_1 = C_1 + C_2$, and p_2, $p_3 = -(C_1+C_2)/2 \pm j\sqrt{3}/2(C_1 - C_2)$, where

$$C_1 = \sqrt[3]{-1/\beta^2 + \sqrt{1/\beta^4 + 1/(27\beta^6)}} \tag{43}$$

$$C_2 = \sqrt[3]{-1/\beta^2 - \sqrt{1/\beta^4 + 1/(27\beta^6)}} \tag{44}$$

Because C_1 and C_2 are both real, p_1 will be real, and p_2, p_3 will be complex. The real root is to be used in solving Eq. (41) for the breakaway point. Thus,

$$q_c = \frac{1}{p_1} = \frac{1}{C_1 + C_2} \tag{45}$$

To obtain the value of T_o for breakaway, substitute q_c into Eq. (40):

$$T_o^* = \frac{(q_c+1)\left(q_c^2 - \beta^2\right)}{q_c} \tag{46}$$

Equations (43–46) establish the relationships between β^2 and T_o that define the stability boundary for the undamped case. This boundary is displayed graphically in Fig. 3. The region below the curve is unstable.

Damped Case: $\xi_o > 0$

The characteristic equation becomes one with complex coefficients:

$$C_o(q) + j\xi_o(q - q_\Lambda)(q - q_\Delta) = 0 \tag{47}$$

The quantities q_Λ and q_Δ are introduced as damping roots defined by $q_\Lambda = -1/\Lambda$ and $q_\Delta = -1/\Delta$. For cases of practical interest, δ will be small and positive. The parameter λ can assume values between $+1$ and -1 with negative values corresponding to a prolate

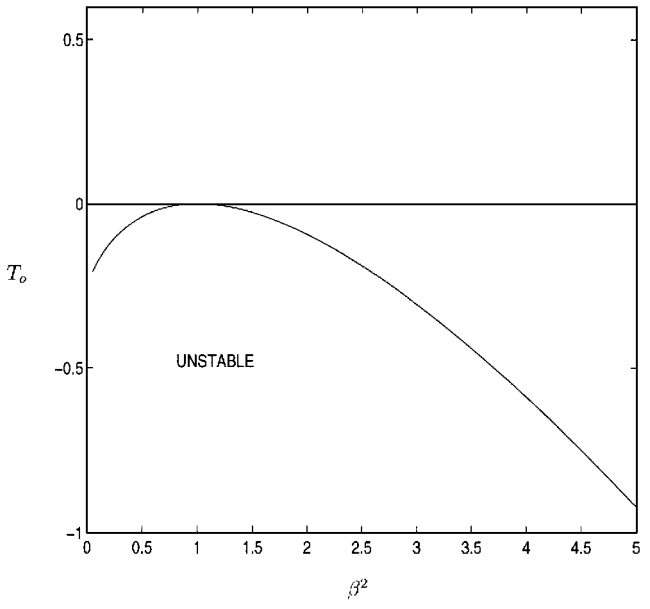

Fig. 3 Instability chart in the absence of damping.

rocket and positive values corresponding to an oblate rocket. Thus for this study, the parameters Λ, Δ, and ξ_o will be positive and the damping roots q_Λ and q_Δ will be negative.

The roots of $C_o(q)$ have been analyzed in the undamped case. The focus here is on the effect of adding the damping term. Consider, first, the case $T_o > T_o^*$ for which $C_o(q)$ has only real roots. If none of the roots are equal to q_Λ or q_Δ, there cannot be any real value of q satisfying both $C_o(q) = 0$ and $(q - q_\Lambda)(q - q_\Delta) = 0$. Equation (47) hence does not have any real solution. The roots of Eq. (47) will all be complex in the presence of damping. Stability conditions can, therefore, be derived assuming infinitesimally small ξ_o. Once a root moves inside the stable (or unstable) region on the q plane at infinitesimal ξ_o, it will stay in that region for all $\xi_o > 0$. The root will not cross over between stable and unstable regions when ξ_o is varied, as that would mean existence of a real root for Eq. (47) at some point.

Denote the roots of $C_o(q)$ by q_i and their complex shifts in the presence of infinitesimal ξ_o by ε_i, $i = 1, 2, 3$. Expressions for ε_i can be obtained by differentiating Eq. (47) with respect to ξ_o and solving for the partial derivative $\partial q/\partial \xi_o$. Keeping only first-order terms in ξ_o, one obtains

$$\varepsilon_i = \left.\frac{\partial q}{\partial \xi_o}\right|_{q_i} \xi_o = -j\xi_o \left.\frac{(q - q_\Lambda)(q - q_\Delta)}{\partial C_o(q)/\partial q}\right|_{q_i} \tag{48}$$

The shifts ε_i will be stabilizing if and only if

$$\left.\frac{(q - q_\Lambda)(q - q_\Delta)}{\partial C_o(q)/\partial q}\right|_{q_i} > 0 \tag{49}$$

for $i = 1, 2, 3$.

Figure 4 shows the function $C_o(q)$ vs q. The positive real root of $C_o(q)$ is designated as q_1 and the negative roots as q_2 and q_3, with $q_2 \geq q_3$. The roots q_2 and q_3 define regions A, B, and C as depicted. From Fig. 4,

$$\left.\frac{\partial C_o(q)}{\partial q}\right|_{q_1} > 0, \qquad \left.\frac{\partial C_o(q)}{\partial q}\right|_{q_2} < 0, \qquad \left.\frac{\partial C_o(q)}{\partial q}\right|_{q_3} > 0 \tag{50}$$

The stability condition of Eq. (49) then becomes

$$(q_1 - q_\Lambda)(q_1 - q_\Delta) > 0 \tag{51}$$

$$(q_2 - q_\Lambda)(q_2 - q_\Delta) < 0 \tag{52}$$

$$(q_3 - q_\Lambda)(q_3 - q_\Delta) > 0 \tag{53}$$

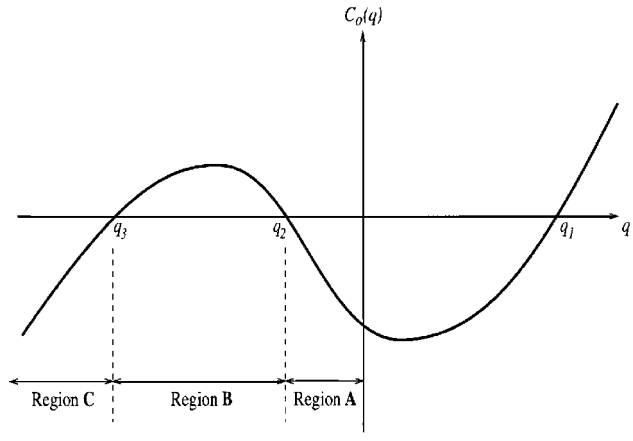

Fig. 4 $C_o(q)$ vs q.

Satisfaction of all three conditions (51–53) are necessary and sufficient for stability.

Condition (51) is always satisfied because q_1 is positive and q_Λ and q_Δ are negative. Condition (52) is satisfied if q_Λ and q_Δ lie separately on the two sides of q_2 in Fig. 4. Condition (53) is satisfied if both q_Λ and q_Δ lie on the right or the left of q_3. Altogether, conditions (51–53) will be satisfied when q_Λ and q_Δ lie separately in regions of A and B. This yields the following stability conditions.

For $\delta < \lambda (q_\Delta < q_\Lambda)$,

$$\begin{aligned} &q_2 < q_\Lambda \ (q_\Lambda \text{ in region A}) \\ &q_3 < q_\Delta < q_2 \ (q_\Delta \text{ in region B}) \end{aligned} \tag{54}$$

For $\lambda < \delta (q_\Lambda < q_\Delta)$,

$$\begin{aligned} &q_2 < q_\Delta \ (q_\Delta \text{ in region A}) \\ &q_3 < q_\Lambda < q_2 \ (q_\Lambda \text{ in region B}) \end{aligned} \tag{55}$$

Conditions (54) and (55) are necessary and sufficient for asymptotic stability when Eq. (47) exhibits no real root. In cases when q_2 or q_3 happen to equal q_Λ or q_Δ, however, Eq. (47) will have real roots. Stability will be marginal at best. Analysis of these cases can be conducted by first factoring out the real roots and then examining the stability of the complex roots assuming infinitesimal ξ_o. (Here, the real roots are independent of ξ_o and will not constitute crossover points between stable and unstable regions.) Stability conditions, which include marginally stable cases, are given by relaxing the inequality signs in conditions (54) and (55) from $<$ to $\leq$.

Turning to the case $T_o < T_o^*$ where $C_o(q)$ has an unstable root to start with, instability is ascertained for infinitesimally small ξ_o. Reasoning as before, it can be concluded that the nominal motion will remain unstable in the presence of damping.

The asymptotic stability conditions can be put in another form, noting from Fig. 4 that $C_o(q) < 0$ for q in A and $C_o(q) > 0$ for q in B.

For $\delta < \lambda \, (q_\Delta < q_\Lambda)$,

$$\begin{aligned} C_o(q_\Lambda) &< 0 \\ C_o(q_\Delta) &> 0 \end{aligned} \tag{56}$$

For $\lambda < \delta \, (q_\Lambda < q_\Delta)$,

$$\begin{aligned} C_o(q_\Delta) &< 0 \\ C_o(q_\Lambda) &> 0 \end{aligned} \tag{57}$$

Equations (56) and (57) can be combined into a compact form,

$$\begin{aligned} (\lambda - \delta)/C_o(q_\Delta) &> 0 \\ C_o(q_\Lambda) C_o(q_\Delta) &< 0 \end{aligned} \tag{58}$$

With $C_o(q) = (q + 1)(q^2 - \beta^2) - T_o q$, one has

$$C_o(q_\Lambda) = \frac{\lambda/(1 + \lambda)^2 - \lambda\beta^2 + T_o}{1 + \lambda} \tag{59}$$

$$C_o(q_\Delta) = \frac{\delta/(1 + \delta)^2 - \delta\beta^2 + T_o}{1 + \delta} \tag{60}$$

Equation (58), therefore, gives the conditions derived in Ref. 11 using the second method of Lyapunov.

There is yet another derivation of the stability conditions, and that is to put Eq. (47) in the root locus form $1 + j\xi_o(q - q_\Lambda)(q - q_\Delta)/C_o(q) = 0$ and examine the angles of departure for q_1, q_2, and q_3 subjected to perturbation $j\xi_o$. This derivation is basically the same as the present approach.

Stability conditions (54) and (55) can be expressed in a useful form if one observes the following.

Stable Coning Condition (SCC): The coning motion is asymptotically stable in the presence of damping if and only if q_2 is the only real root of $C_o(q) = 0$ lying between the damping roots q_Λ and q_Δ, i.e., $(q_2 - q_\Lambda)(q_2 - q_\Delta) < 0$.

Thus, given δ and λ, or q_Δ and q_Λ, the values of T_o for asymptotic stability can be obtained from the root locus of the undamped characteristic values. For $\lambda < \delta$ ($q_\Lambda < q_\Delta$), the upper and lower bounds of T_o for asymptotic stability are given as $T_o^u = T_o(q_\Delta)$ and $T_o^l = T_o(q_\Lambda)$, where the function $T_o(q)$ is given by Eq. (40). For $\delta < \lambda (q_\Delta < q_\Lambda)$, the bounds are reversed with $T_o^u = T_o(q_\Lambda)$ and $T_o^l = T_o(q_\Delta)$. The stability boundaries can be obtained by plotting the straight lines $T_o(q_\Lambda) = \lambda\beta^2 - \lambda/\Lambda^2$ and $T_o(q_\Delta) = \delta\beta^2 - \delta/\Delta^2$ in the T_o vs β^2 plane. Figure 5 shows the stability region when $\lambda < \delta$ and Fig. 6 shows the region when $\lambda > \delta$. The stability boundary

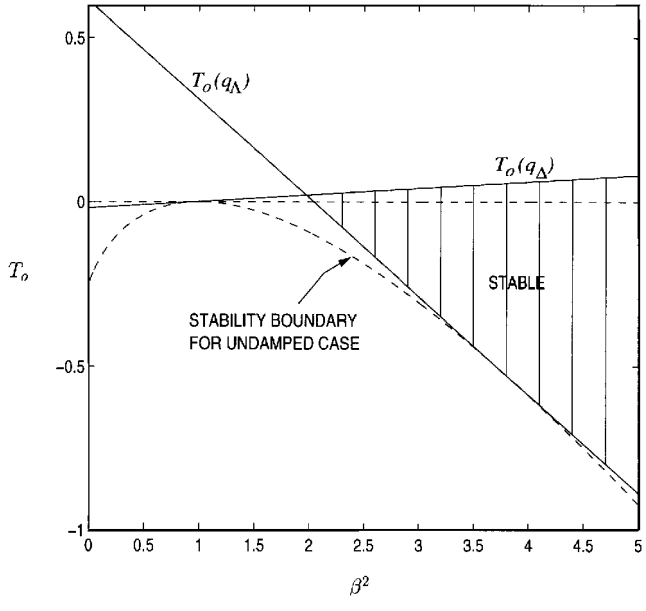

Fig. 5 Stability chart in the presence of damping: $\lambda < \delta$.

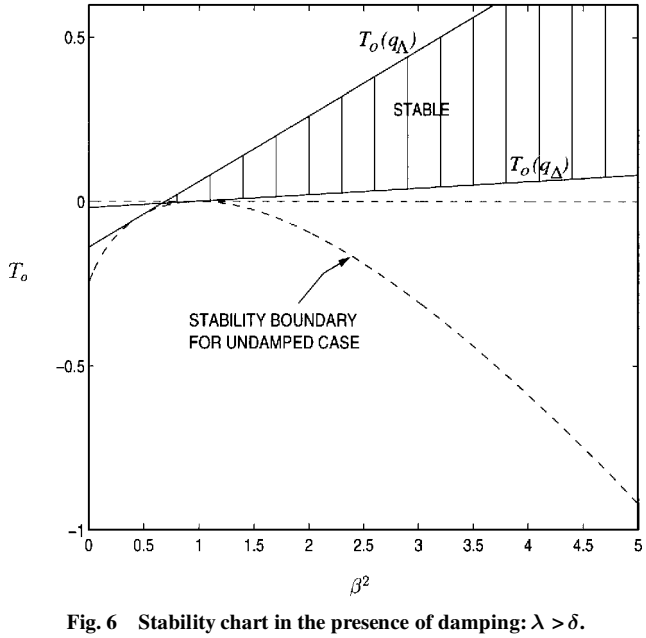

Fig. 6 Stability chart in the presence of damping: $\lambda > \delta$.

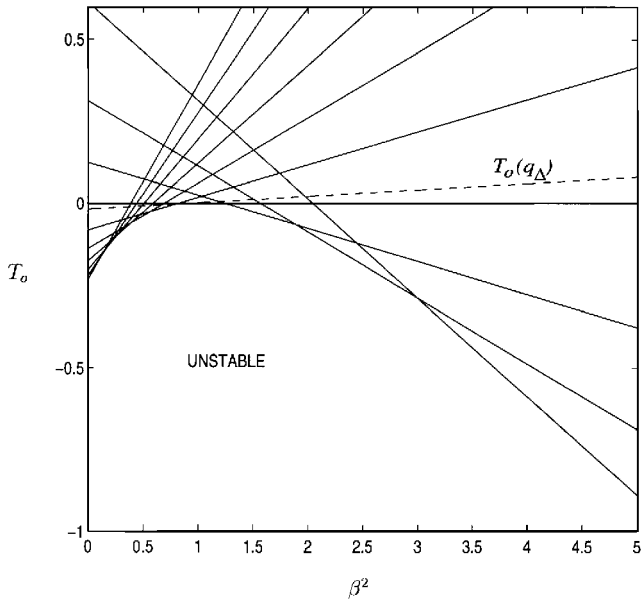

Fig. 7 Stability chart with damping showing accumulation of λ lines.

T_o^* for the undamped case is also included for comparison. A closer examination of Fig. 5 will be given later. The stability regions are bounded by two lines with slopes δ and λ originating from a vertex. The boundaries of the stability regions constitute the regions of marginal stability. Remaining areas in the figures are the regions of instability. The vertex coordinates on the T_o vs β^2 plane can be obtained from the expressions of $T_o(q_\Lambda)$ and $T_o(q_\Delta)$: $\beta^2 = (1 - \delta\lambda)/(\Lambda^2\Delta^2)$, $T_o = -\delta\lambda(\Lambda + \Delta)/(\Lambda^2\Delta^2)$.

In Fig. 7 the value of δ is held fixed at 0.02, and λ is allowed to vary through a sequence of positive and negative values. It is seen that the resulting $T_o(q_\Lambda)$ lines are tangent to T_o^*, and as more of these lines are plotted, the stability curve of the undamped case clearly emerges.

To examine Fig. 5 more closely, the root locus in Fig. 2 is referred. The damping roots q_Λ and q_Δ lie on the negative real axis with $q_\Lambda < q_\Delta$ ($\lambda < \delta$ case). Imagine that T_o is being decreased from a large (positive) value, and consequently, q_2 is moving from somewhere near the origin toward the left and q_3 is moving from near $-\infty$ toward the right. The critical point q_c where q_2 and q_3 meet depends on β^2 [Eq. (45)]. If β^2 is relatively large so that q_c lies on the left of q_Λ, then q_3 will not enter the range (q_Λ, q_Δ) at all. Stability is dictated by the points where q_2 reaches q_Δ and enters the range (q_Λ, q_Δ) on the right validating the SCC and where q_2 reaches q_Λ and exits the range (q_Λ, q_Δ) on the left invalidating the SCC. The upper and lower bounds on T_o are obtained by substituting q_Δ and q_Λ into Eq. (40), which leads to $T_o^u = T_o(q_\Delta)$ and $T_o^l = T_o(q_\Lambda)$. Moreover, if β^2 is such that $q_c = q_\Lambda$, $T_o^l = T_o(q_c) = T_o^*$ [Eq. (46)]. The lower bound T_o^l touches the undamped stability boundary at this point. If β^2 is smaller so that q_c lies to the right of q_Λ, the upper bound remains dictated by where q_2 reaches q_Δ and enters the stability range (q_Λ, q_Δ) on the right, but the lower bound will be dictated by where q_3 reaches q_Λ and enters the range (q_Λ, q_Δ) on the left invalidating the SCC. The resulting expression for T_o^l, though, remains as $T_o^l = T_o(q_\Lambda)$. Furthermore, if β^2 is relatively small such that $T_o(q_\Lambda) > T_o(q_\Delta)$, the root q_3 actually enters (q_Λ, q_Δ) before q_2. Then the stability condition is always violated and there is no stabilizing value for T_o. These observations account for the various features of Fig. 5. A similar interpretation applies to Fig. 6.

In the region above the stability curve of Fig. 3, the stability investigation of Ref. 2 was inconclusive. The situation in this region is clarified by Ref. 11 and the present analysis. It is seen that in this region the addition of damping sometimes produces asymptotic stability and sometimes produces instability. This type of behavior is characteristic of many rotational dynamics problems including the problem of torque free motion. Moreover, the result suggests that a passive device may be added to a spinning rocket that will enhance its stability. This capability was demonstrated in Refs. 13 and 14.

The stability charts for the damped case can be further simplified. The ranges of T_o for asymptotic stability can be observed from Figs. 5 and 6 to be as follows: if $\lambda < \delta$ and $T_o(q_\Delta) > T_o(q_\Lambda)$, then $T_o(q_\Delta) > T_o > T_o(q_\Lambda)$, and if $\lambda > \delta$ and $T_o(q_\Delta) < T_o(q_\Lambda)$, then $T_o(q_\Delta) < T_o < T_o(q_\Lambda)$. Substituting $T_o(q_\Lambda) = \lambda\beta^2 - \lambda/\Lambda^2$, $T_o(q_\Delta) = \delta\beta^2 - \delta/\Delta^2$, and $T_o = \delta\beta^2 + T/\Lambda^2$ [Eq. (29)] into these expressions yields the following.

If $\lambda < \delta$ and $-\delta/\Delta^2 > (\lambda - \delta)\beta^2 - \lambda/\Lambda^2$, then

$$-\delta/\Delta^2 > T/\Lambda^2 > (\lambda - \delta)\beta^2 - \lambda/\Lambda^2 \tag{61}$$

If $\lambda > \delta$ and $-\delta/\Delta^2 < (\lambda - \delta)\beta^2 - \lambda/\Lambda^2$, then

$$-\delta/\Delta^2 < T/\Lambda^2 < (\lambda - \delta)\beta^2 - \lambda/\Lambda^2 \tag{62}$$

Defining a new parameter $J = (T/\Lambda^2 + \delta/\Delta^2)/(\lambda - \delta)$, Eqs. (61) and (62) then reduce to a single inequality. For stability we require

$$J^l = 0 < J < J^u = \beta^2 - (1 - \delta\lambda)/(\Lambda^2\Delta^2) \tag{63}$$

The quantities J^l and J^u are the lower and upper bounds of J for asymptotic stability. As a result, the stable region in the J vs β^2 plane is bounded by straight lines with slopes of 1 and 0 originating from a vertex at $[(1-\delta\lambda)/(\Lambda^2\Delta^2), 0]$. In this case, a single stability chart applies to both cases $\lambda < \delta$ and $\lambda > \delta$.

Discussion and Application

The previous sections present the stability analysis of an idealized problem. No approximations have been made except for linearizing the governing equations. All parameters, including the mass of the system, have been presumed constant. In the rocket problem, which motivated the study, of course, the parameters are not constant, and the system does lose mass. An analysis that correctly takes account of these variations would be much more complicated than that presented so far and much insight would be lost. To retain the simplicity of the present treatment, we argue that if the parameters change slowly with respect to the period of a single spin cycle, the analysis can be used to study the qualitative behavior of the system as the mass properties vary. Proceeding in this spirit, one first determines how λ, T, δ, β^2, and various parameters vary over the time interval of interest. Then the stability conditions can be used to check whether the parameters lead to instability at any time during this interval.

As an example, assume that the spacecraft mass properties I_1, I_3, M, and h are varying linearly in time during the burn. Specifically, let I_1 decrease from 2712 kg·m^2 at time $t = 0$ to 868 kg·m^2 at time $t = 85$ s, and let I_3 decrease from 813 to 468 kg·m^2 during the same period. The behavior of Λ, which is dominated by I_1 and I_3, hence, varies from 0.3 at $t = 0$ to 0.55 at $t = 85$ s. The rocket is always prolate, but it becomes less so as the burn proceeds. Also, let the spacecraft mass M vary from 3284 to 1940 kg during the interval, and let h start out at -0.2 m at $t = 0$ and decrease to -0.5 m at the end of the burn as the loss of rocket fuel moves the system mass center toward the front of the rocket. The thrust force and spin rate are given by $F = 66{,}723$ N and $\Omega = 2\pi$ rad/s. Except for h, these assumed values are the same as those utilized in the numerical example of Ref. 2 for the undamped case and are derived largely from actual rocket data. The example in Ref. 2 also assumed $m = 131$ kg and $\gamma^2 = 0.25$ throughout the burn. It was pointed out that m and γ^2 are very difficult to determine. Here, we delay assigning values for m and γ^2 until later. We can, however, safely assume that m is relatively small (up to only a few percent of M) and, hence, δ is small and positive. As λ is negative (the spacecraft is prolate), only the $\lambda < \delta$ case needs to be considered in this example. Substituting Eq. (31) into Eq. (61), we obtain the following requirement for stability:

$$-\delta\Lambda^2/\Delta^2 > T > (\lambda - \delta)\gamma^2 - \lambda \tag{64}$$

Equation (64) can be viewed as consisting of two parts, $-\delta\Lambda^2/\Delta^2 > T$ and $T > (\lambda - \delta)\gamma^2 - \lambda$, both of which need to be satisfied for stability. Substituting Eqs. (15) and (16) for δ and T, the first part becomes

$$-\Lambda^2/\Delta^2 > F/[(M + m)h\Omega^2] \tag{65}$$

The left-hand side of Eq. (65) is basically equal to $-\Lambda^2$ since $\Delta = 1 + \delta \approx 1$. The right-hand side depends primarily on F and Ω, which we know with some certainty, and the assumed time histories of M and h. The internal mass m plays a relatively minor role in this equation as it is small compared to M. When h is positive, the right-hand side of Eq. (65) is positive and the left-hand side is negative. Hence, Eq. (65) is not satisfied, and the system is unstable. If m represents liquid sloshing in fuel tank, it may be possible for h to be positive. Here, we focus on the case where m represents liquid slag and, hence, h is always negative. Substituting the parameters as assumed shows that Eq. (65) is satisfied during the whole duration of the burn. After the burn, however, $F = 0$ and the right-hand side of Eq. (65) becomes zero. Hence, Eq. (65) is violated, and the system is unstable. This agrees with the known behavior of a dissipative torque free body, which is unstable if the body is prolate.

The second part of Eq. (64) can be rewritten to yield a stable range for γ^2,

$$(T + \lambda)/(\lambda - \delta) < \underline{\gamma}^2 \tag{66}$$

where the fact $(\lambda - \delta) < 0$ has been used. Equation (66) yields a lower bound of γ^2 for satisfying the stability condition. Figure 8 depicts this bound, $\underline{\gamma}^2 = (T + \lambda)/(\lambda - \delta)$, over the burn interval for the assumed time histories and slag mass of $m = 40$, 60, and 80 kg. The bound attains values close to unity as both T and δ are small compared to λ. Since $\gamma^2 = k/[m(1-\mu)\Omega^2]$, this indicates that resonance between internal mass oscillation $[\sqrt{(k/m)}]$ and nominal spin rate Ω is needed to produce the observed coning instability. Figure 8 shows that if $\gamma^2 = 1.01$, say, instability will occur around 54 s into the burn if the sloshing mass $m = 80$ kg. Instability will occur at 64 and 74 s into the burn, if $m = 60$ and 40 kg, respectively. Given the time for onset of coning instability, Fig. 8 can be used to infer a relation between m and γ^2.

We now calculate the system root loci by assuming that m grows linearly from zero at $t = 0$ to 60 kg at $t = 85$ s. We implicitly assume that the sloshing mass model is valid throughout the burn. In reality, the model may become a viable description of the spacecraft dynamics only after sufficient mass has accumulated. Based on Fig. 8, we choose a value of 1.01 for γ^2. Figure 9 shows the system roots of Eq. (35) for the duration of the burn. There is a third root residing well into the left-half plane, which is not included in the figure. Figure 9 shows that the system is stable at the beginning of the burn. At approximately $t = 57$ s, however, one of the roots moves into the unstable region. The growth rate of this root increases appreciably from $t = 57$ s until the end of burn at $t = 85$ s. At this point, the thrust force F ceases and the system roots attain locations as indicated by the circles. There is still an unstable root

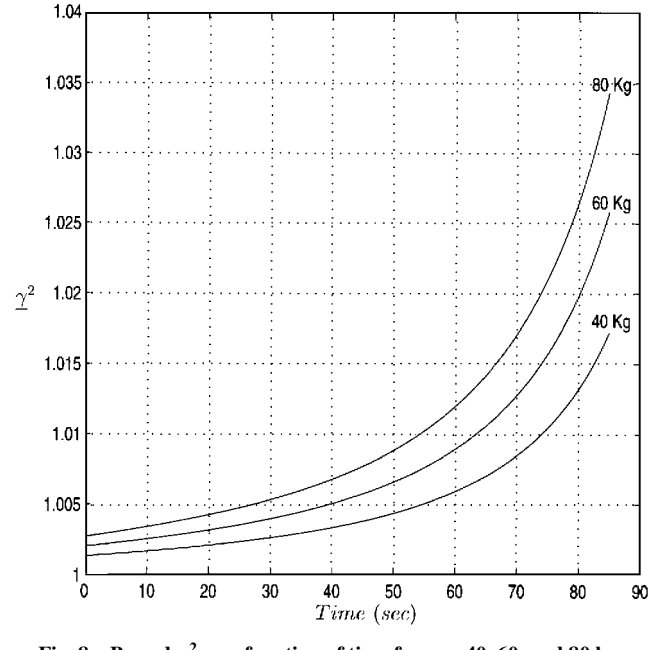

Fig. 8 Bound $\underline{\gamma}^2$ as a function of time for m = 40, 60, and 80 kg.

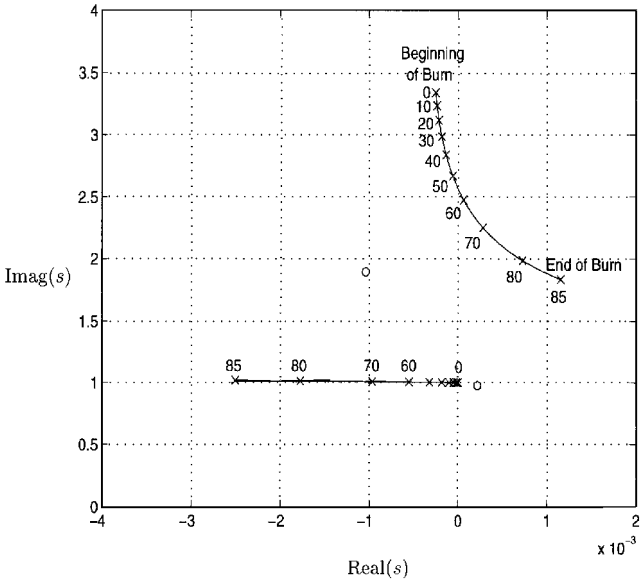

Fig. 9 System root loci during the burn.

but the growth rate is much reduced. The behavior, as outlined here, is in qualitative agreement with that observed in space.

In this example, the parameter ξ_o is held fixed at 0.2. A different value for ξ_o will change the scalings of the axes but not the qualitative characteristics of Fig. 9. The damping coefficient of the internal mass is $\rho = \frac{1}{2}(c/m)/\sqrt{(k/m)}$. Upon substitution of Eqs. (12), (13), and (30), $\rho = \sqrt{(1-\mu)}\Lambda\xi_o/(2\gamma\Delta)$. With $\gamma \approx 1$, $\Delta \approx 1$, and Λ varying from 0.3 to 0.55 during the interval, the corresponding damping coefficient varies from about 3% at the beginning to 5.5% at the end of burn. One can also set a constant value for ρ throughout the burn, in which case ξ_o will be time varying instead.

Conclusions

The problem considered in this paper and the referenced works may be viewed as an extension of the freely spinning body problem wherein a new ingredient has been added: the thrust vector that acts along the symmetry axis. Nominally the thrust vector produces no torque about the mass center, but when there is internal mass motion, the mass center can move off the thrust axis producing an external torque.

This system is nonconservative even in the absence of dissipative forces. Clearly, the thrust vector can add energy to the system. The stability of such a system without dissipative forces was studied in an earlier work, and a substantial region of instability was found. A follow-up work further examined how the stability regions are modified when dissipative forces are added to the model. By using the direct method of Lyapunov, it was possible to obtain analytical stability conditions that are necessary and sufficient for stability. The present work provides an alternative derivation of the stability conditions based on a perturbation analysis of the undamped characteristic values. The results provide additional insight into the stability charts. Compared to the undamped case, the findings for the dissipative case include the following.

1) It was found that regions that were unstable in the absence of dissipative forces remain so when dissipative forces are added. In areas where the undamped stability results were inconclusive, some regions become unstable and some become asymptotically stable. Thus, the region of instability in the presence of dissipative forces is larger than that found for purely elastic systems. Similar results have been found previously when the stability of rotating systems is studied with and without dissipative forces.

2) For the undamped case, instability can only occur when the moving internal mass is aft of the system mass center. This is not true for the dissipative case. From the stability conditions, one can deduce that instability may arise for h positive or negative. The moving mass need not be aft of the system mass center to cause instability.

3) When dissipation is added, it becomes clear that internal mass motion can both enhance stability and exacerbate instability. This suggests that a passive device can be added to a spinning rocket that will enhance its stability.

4) The maximum axis spin rule does not apply in the presence of axial thrust.

This paper also includes a numerical example demonstrating how the present analysis can be used to examine the stability of a time varying spacecraft system. The example shows that coning growth at the later stage of the burn similar to that observed in space is possible assuming certain time histories of spacecraft parameters.

References

[1]Flandro, G. A., Leloudis, M., and Roach, R., "Flow Induced Nutation Instability in Spinning Solid Propellant Rockets," U.S. Air Force Astronautics Lab. (AFSC), AL-TR-89-084, April 1990.

[2]Mingori, D. L., and Yam, Y., "Nutational Instability of a Spinning Spacecraft with Internal Mass Motion and Axial Thrust," *Proceedings of the AIAA/AAS Astrodynamics Conference* (Williamsburg, VA), AIAA, Washington, DC, 1986, pp. 367–375 (AIAA Paper 86-47901).

[3]Or, A. C., "Rotor-Pendulum Model for the Perigee Assist Module Nutation Anomaly," *Journal of Guidance, Control, and Dynamics*, Vol. 15, No. 2, 1992, pp. 297–303.

[4]Or, A. C., "Stability of Spinning Spacecraft Containing Shallow Pool of Liquid Under Thrust," *Journal of Guidance, Control, and Dynamics*, Vol. 17, No. 5, 1994, pp. 1019–1027.

[5]McIntyre, J. E., and Tanner, T. M., "Fuel Slosh in a Spinning Propellant Tank: An Eigenmode Approach," *Space Communication and Broadcasting*, Vol. 5, No. 4, 1987, pp. 229–251.

[6]Staunton, B. D., and Mingori, D. L., "Attitude Dynamics of Spinning Rockets in Space with Internal Fluid Motion," *Proceedings of the AIAA Guidance, Navigation, and Control Conference* (Monterey, CA), AIAA, Washington, DC, 1993, pp. 507–516 (AIAA Paper 93-3758).

[7]Cochran, J. E., Jr., and Kang, J. Y., "Nonlinear Stability Analysis of the Attitude Motion of a Spin-Stabilized Upper Stage," *Proceedings of the AAS/AIAA Spaceflight Mechanics Meeting* (Houston, TX), 1991, pp. 354–364 (AAS Paper 91-109).

[8]Kang, J. Y., and Cochran, J. E., Jr., "Further Investigations of Anomalous Attitude Motion of Spin-Stabilized Upper Stages," *Proceedings of the AAS/AIAA Astrodynamics Specialist Conference* (Durango, CO), 1991, pp. 705–722 (AAS Paper 91-480).

[9]Hughes, P. C., *Spacecraft Attitude Dynamics*, Wiley, New York, 1986, Chaps. 3 and 4.

[10]Chinnery, A. E., and Hall, C. D., "Motion of a Rigid Body with an Attached Spring-Mass Damper," *Journal of Guidance, Control, and Dynamics*, Vol. 18, No. 6, 1995, pp. 1404–1409.

[11]Mingori, D. L., Halsmer, D. M., and Yam, Y., "Stability of Spinning Rockets with Internal Mass Motion," *Proceedings of the AAS/AIAA Spaceflight Mechanics Meeting* (Pasadena, CA), 1993, pp. 199–209 (AAS Paper 93-135).

[12]Bolotin, V. V., *Nonconservative Problems in the Theory of Elastic Stability*, Macmillan, New York, 1963, pp. 7–15, 47, 48.

[13]Halsmer, D. M., and Mingori, D. L., "Nutational Stability and Passive Control of Spinning Rockets with Internal Mass Motion," *Journal of Guidance, Control, and Dynamics*, Vol. 18, No. 5, 1995, pp. 1197–1203.

[14]Halsmer, D. M., "Nutational Stability and Passive Control of Symmetric Spinning Bodies with Axial Forcing and Internal Mass Motion," Ph.D. Dissertation, Mechanical, Aerospace, and Nuclear Engineering Dept., Univ. of California, Los Angeles, CA, 1992.